The Treatment of Muscle Atrophy After Rotator Cuff Tears Using Electroconductive Nanofibrous Matrices

Xiaoyan Tang [1,2,3,4] · Nikoo Saveh Shemshaki [1,2,4,5] · Varadraj N. Vernekar [1,2,4] · Anupama Prabhath [1,2,4,5] ·
Emmanuel Kuyinu [1,2,4] · Ho-Man Kan [1,2,4] · Mohammed Barajaa [1,2,4,5] · Yusuf Khan [1,2,3,4,5] · Cato T. Laurencin [1,2,3,4,5,6,7]

Abstract

Rotator cuff tears (RCTs) are a common cause of disability and pain in the adult population. Despite the successful repair of the torn tendon, the delay between the time of injury and time of repair can cause muscle atrophy. The goal of the study was to engineer an electroconductive nanofibrous matrix with an aligned orientation to enhance muscle regeneration after rotator cuff (RC) repair. The electroconductive nanofibrous matrix was fabricated by coating poly(3,4-ethylenedioxythiophene):poly(styrenesulfonate) (PEDOT:PSS) nanoparticles onto the aligned poly(ε-caprolactone) (PCL) electrospun nanofibers. The regenerative potential of the matrix was evaluated using two repair models of RCTs namely acute and sub-acute. Sprague–Dawley rats ($n = 39$) were randomly assigned to 1 of 8 groups. For the acute model, the matrix was implanted on supraspinatus muscle immediately after the injury. The repair surgery for the sub-acute model was conducted 6 weeks after injury. The supraspinatus muscle was harvested for histological analysis 2 and 6 weeks after repair. The results demonstrated the efficacy of electrical and topographical cues on the treatment of muscle atrophy in vivo. In both acute and sub-acute models, the stimulus effects of topographical and electrical cues reduced the gap area between muscle fibers. This study showed that muscle atrophy can be alleviated by successful surgical repair using an electroconductive nanofibrous matrix in a rat RC model.

Lay Summary and Future Work

Rotator cuff tears of the shoulder are a common cause of pain and disability, and available treatments focus on minimizing pain as well as restoring function of the shoulder. In clinical settings, the success of either sub-acute or chronic rotator cuff tendon repair can be compromised by muscle functionality. This study showed the efficacy of an electroconductive nanofibrous matrix to reverse muscle atrophy after successful surgical repair in rat acute and sub-acute rotator cuff model. Future study will investigate the regenerative potential of the engineered matrix in a chronic rotator cuff tear model.

Keywords Rotator cuff · Electroconductive matrix · Nanofibers · Muscle atrophy

Introduction

Rotator cuff tears (RCTs) are a common cause of disability and pain in the adult population [1–4]. Tendon detachment can cause tendon retraction, fatty infiltration, muscle atrophy, and subsequently shoulder instability and dysfunction [3, 5, 6]. A critical hurdle of repairing massive RCTs is the high re-tear rate (up to 94%) after repair [3]. Several factors, such as patient age, tear size, muscle atrophy, delayed repair, and repair strategies, influence the rate of re-tear [3, 7–12].

One of the challenges of rotator cuff (RC) repair is the commonly observed delay between the time of injury and surgical repair [13]. The medical terms of acute, sub-acute, and chronic are being used as references to the delay between the time of injury and repair. Acute RC injury refers to the incision that will be repaired in a short time; in humans, it could be a few days or maybe weeks. The injury will be considered chronic if the torn RC is persisting for a prolonged period. On the other hand, sub-acute injuries indicate the conditions that have passed the acute phase but are not yet chronic.

Sub-acute and chronic RCTs are often associated with a set of pathological changes that include muscle atrophy, smaller muscle cross-sectional area, fatty infiltration, and fibrosis [14, 15]. In the initial days post-injury, the migration of inflammatory cells leads to apoptosis of muscle fibers [16, 17]. The intrinsic degenerative

✉ Cato T. Laurencin
Laurencin@uchc.edu

Extended author information available on the last page of the article

changes of the musculotendinous unit lead to muscle atrophy [18, 19]. Despite successful repair of the torn tendon, muscle atrophy is an issue that adversely affects RCTs healing in sub-acute and chronic tears [20]. The undesirable outcomes associated with current surgical techniques have motivated tissue regenerative engineering approaches for RC healing. Regenerative engineering is a novel, alternative approach using the convergence of advanced materials science, stem cell research, physical sciences, and areas of developmental biology and clinical translation that has the potential to address muscle degeneration in moderate injuries with minimal to no scar formation and may also offer a regeneration strategy in the case of severe injuries [21–27].

Biomimetic matrices with similar structures to native muscle can facilitate the regeneration of muscle [28]. Nanostructure-based matrices such as polymeric/non-polymeric nanofibers, nanotubes, and nanoparticles are considered promising materials in tissue regenerative engineering [29, 30]. Among different nanostructures, nanofibers are one of the most interesting materials owing to their continuous nanoscale long fibers [3, 4, 31–34]. The nanofiber-based structures showed the most similarity to native muscle tissue by providing similar structures and appropriate mechanical properties. Since muscle is an electrically excitable tissue, the combination of electroconductive material along with aligned nanofibers significantly improves interactions between materials and cells and facilitates myoblast communication, growth, and development [4, 28, 35–37].

So far, many studies evaluated the potential of electroconductive materials to promote muscle growth and differentiation in vitro [4, 38–40]. According to the literature, the regenerative potential of electroconductive matrices has not been extensively investigated for healing muscle atrophy after RCTs in an animal model. In this study, the efficacy of electrical and topographical cues on reducing muscle atrophy was investigated through implanting electroconductive nanofibrous matrix on supraspinatus muscle after successful RC repair. The aligned poly(ε-caprolactone) (PCL) nanofibers were fabricated by electrospinning technique; then, the electrospun layers were coated with poly(3,4-ethylenedioxythiophene):poly(styrenesulfonate) (PEDOT:PSS) nanoparticles. The efficacy of the matrix was investigated in both acute and sub-acute RCT models. At 2 and 6 weeks post-repair, the supraspinatus muscle was harvested for histological analysis.

Materials and Methods

Matrix Preparation

Matrix design, fabrication, and characterization were published elsewhere (Fig. 1B) [4]. Briefly, the aligned nanofibers were fabricated by electrospinning using 15% (w/v) polycaprolactone (PCL, from Sigma-Aldrich) solution in ethanol and methylene chloride (15:85 ratio, from Sigma-Aldrich), with a 2.5 mL/min flow rate and 1 kV/cm potential at ambient temperature and humidity. Dopamine hydrochloride (2 mg/mL, average molecular weight 8000 Da, from Sigma-Aldrich) was coated onto the matrices for 24 h at pH 8.5 (DOPA/PCL) [41]. The modified DOPA/PCL matrices were washed, dried, and subsequently coated with 30 μL of 10% poly (3,4-ethylenedioxythiophene)-polystyrene sulfonate (PEDOT:PSS 1:2.5, from Sigma-Aldrich) in PBS (PEDOT:PSS/DOPA/PCL). The coated matrices were dried for 48 h under vacuum and sterilized using 70% ethanol and UV for half an hour/side.

Surgical Procedure

The surgical groups and numbers are listed in Fig. 1A. Acute and sub-acute models were developed using adult male Sprague–Dawley rats (Charles River Laboratories, Inc.) weighing between 400 and 450 g. All animal experiments were performed following protocols approved by the Institutional Animal Care and Use Committee (IACUC) at the University of Connecticut (Protocol number: 101417-0919).

The rats were housed in a controlled environment on a light/dark cycle and fed with standard rodent chow and water. An open surgical approach was followed to create a full-thickness RCT of the supraspinatus tendon in the left shoulder. This was followed by a surgical repair with or without the insertion of PEDOT: PSS matrix. Anesthesia was induced with isoflurane (2–3%) and maintained through a facemask for both procedures. After skin incision, a longitudinal incision was made on the deltoid muscle to expose the RC tendon at the shoulder joint. The supraspinatus tendon was completely detached from the bone–tendon insertion on the humeral head, marked with a 5–0 Prolene suture (Ethicon, Johnson & Johnson Medical Ltd.) at the musculotendinous junction, and allowed to retract.

Acute Surgery Procedure Immediately after the injury, a tunnel was created in the cortical bone under the insertion of the supraspinatus tendon and surgical reattachment of the tendon was performed. For the surgical repair with matrix groups (RM), a 0.6 cm (length) × 0.3 cm (width) electroconductive nanofibrous matrix was sutured on the belly of the supraspinatus muscle; then, the overlying tissue and skin were closed. Analgesia (buprenorphine, 0.05–0.1 mg/kg) and antibiotic (sulmethaoxole and trimethoprim 40 mg/mL and 8 mg/mL) were administered according to the protocol, and the rats were kept under heat lamps until they were transferred to their cages.

Sub-acute Surgery Procedure The tendon tear was created as described above, and the surgical site closed. The second
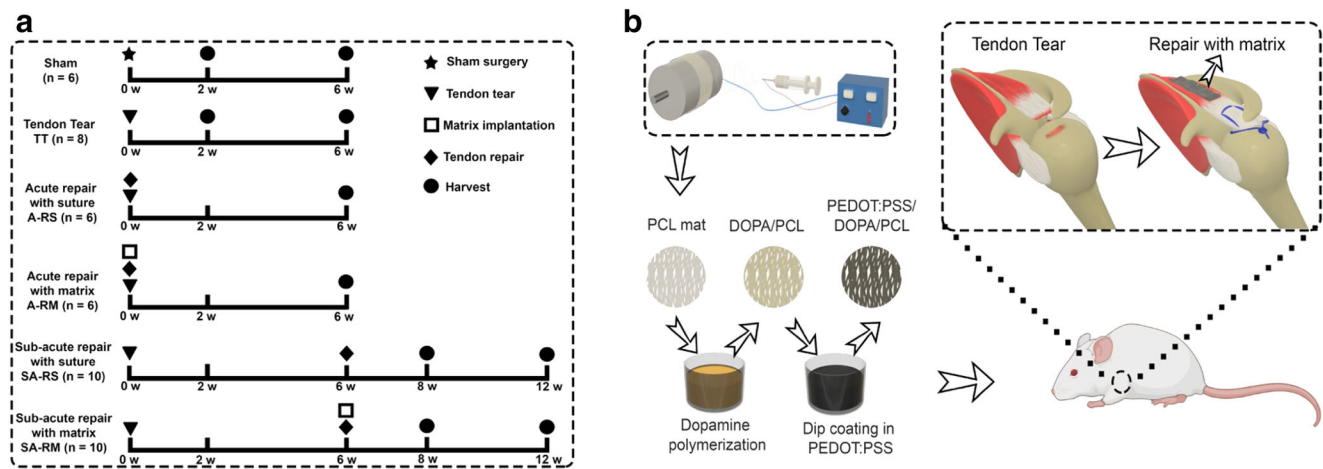
Fig. 1 (**A**) Diagram of experimental groups. For sub-acute groups, 4 and 6 rats were sacrificed 2 and 6 weeks after repair respectively; (**B**) schematic illustration of the rotator cuff surgery model. The aligned PCL nanofibers were fabricated by electrospinning technique. Following the electrospinning, dopamine was applied onto the PCL

fibers to polymerize and form a polydopamine coating. DOPA/PCL surfaces were washed, dried, and coated with 10% PEDOT:PSS. Following the surgical repair of the torn supraspinatus tendon, the matrix was implanted on top of the supraspinatus muscle in both acute and sub-acute models

operation to reattach the tendon was performed 6 weeks after the injury as described in the acute surgery procedure.

Tissue Analysis

Tissue Harvest Rats were sacrificed 6 weeks after surgery for acute groups and 2 and 6 weeks post-surgery for sub-acute groups. The supraspinatus muscles of both the surgical site and the control side (right shoulder) were harvested. The wet mass of the supraspinatus

muscle was weighed immediately. After the measurement, the harvested muscle was used for paraffin embedding.

Wet Weight Measurement The wet mass of the supraspinatus muscle was measured with the use of a digital scale immediately after dissection (Ohaus® Voyager Pro balance). The relative weight change was calculated to show the weight difference between the groups. The weight change percentage was calculated as follows:

$$\text{Relative percentage weight loss} = \left(\frac{\text{supraspinatus weight of the right shoulder} - \text{supraspinatus weight of the left shoulder}}{\text{supraspinatus weight of the left shoulder}}\right) \times 100$$

Immunochemistry Analysis Following an existing protocol, 10-μm sections were rehydrated in phosphate-buffered saline (PBS), fixed in 4% paraformaldehyde, washed in PBS, and immersed in 5% normal donkey serum for 15 min [42]. Tissue sections were imaged and quantified using immunohistochemistry for the fast type II myosin heavy chain (MHC) isoform, slow type I MHC isoform (Novocastra™ Lyophilized Mouse Monoclonal Antibody Myosin Heavy Chain (fast and slow), 1:10; Leica Biosystems and CD31 (Abcam) using fluorescence labeling methods) [42].

Histological Analysis The sections were stained by Masson's trichrome staining, and hematoxylin and eosin to identify fibrotic tissue and muscle fiber outlines [42]. Images were captured and digitized (DM4000B Leica Upright Microscope; Leica Microsystems) at varying magnifications.

Muscle Cross-sectional Area Quantification Sections were visualized at × 10 magnification (Leica Microsystems), and images were recorded using a digital camera. For Masson's trichrome staining, the cross-sectional areas of all muscle fibers were counted. For fast muscle staining, the cross-sectional areas of fifty random muscle fibers per image (6 to 9 images per group) were selected and measured using ImageJ software (National Institutes of Health). Muscle samples were analyzed in a random order, random selection, and the investigator was blinded as to which muscle was being analyzed.

Muscle Gap Quantification Gap areas were quantified between muscle fascicles. Nine representative images with 350 μm × 350 μm dimensions were selected from each group, and ImageJ analysis was used to quantify the muscle gap area.

4

Regen. Eng. Transl. Med. (2021) 7:1–9

Statistical Analysis Mean and standard deviation were expressed as means ± SD. Power analysis was used to determine the number of animals. It is the first time the muscle atrophy in rotator cuff model was studied with matrix implantation. Preliminary data to see the statistical difference was based on volumetric muscle loss (VML) with matrix implantation. Differences between groups were analyzed using one-way ANOVA followed by the Tukey pairwise comparison test, and the difference of $P < 0.05$ was considered statistically significant.

Results

Figure 2 shows the supraspinatus muscle weight loss of acute and sub-acute groups 2 and 6 weeks after surgery. The TT/2w and TT/6w groups showed significant differences compared with sham, acute, and sub-acute repair groups 2 and 6 weeks after repair. There was no significant difference between the suture and matrix repair groups in both acute and sub-acute models. Moreover, no significant differences were observed between sub-acute repair groups after 2 weeks compared with the 6-week groups after repair.

Figure 3A shows H&E staining of the supraspinatus muscle in both acute and sub-acute groups. The images demonstrated the formation of fat cells between muscle fibers in the TT/6w group after detachment. The significant fat formation can be observed in TT/6w compared with TT/2w showing the adverse effects of delayed repair after RCT. All repair groups presented muscle growth compared with the TT/6w group. According to Fig. 3, A-RM and SA-RM/6w exhibited similar muscle fiber integrity to the sham group.

Consistent with H&E results, Masson's trichrome staining (Fig. 3B) showed similar dense packing and integrity of muscle fibers in sham, A-RM, SA-RM/2w, and SA-RM/6w groups. The presence of fibrosis was observed in A-RS, SA-RS/2w, and SA-RM/2w, and TT group showed more fibrosis 6 weeks after detachment.
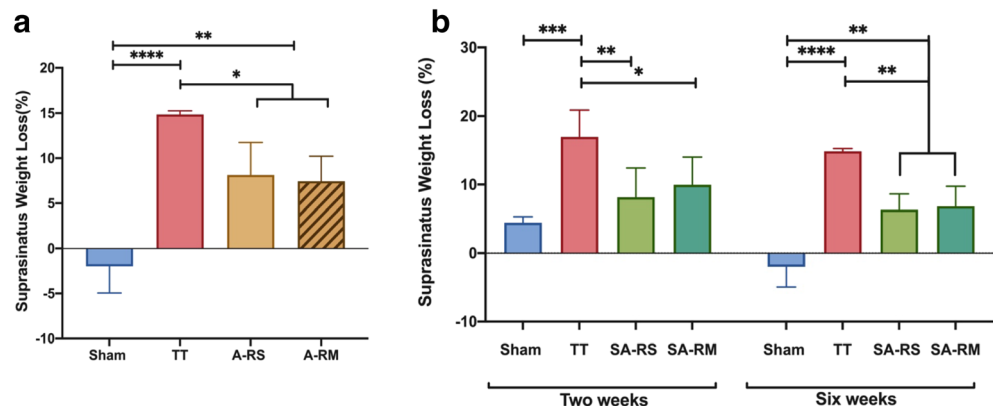
The immunohistochemistry of myosin heavy chain (MHC) was further evaluated for supraspinatus muscle to analyze muscle fiber size and cross-sectional area. According to MHC classification, MHC I and MHC II correspond to muscle fiber type I (slow muscle type) and type II (fast muscle type) [43]. Figure 3C shows the muscle fiber staining of all groups while MHC II fibers show brown color and MHC I fibers show white color. The TT groups presented the minimum quantity of slow muscle fibers. Based on the images, both muscle fibers were observed in all repair groups, but the majority of the muscle fibers were MHC II. The traces of fast muscle fibers ingrowth were observed along with the edges of the matrix, 2 and 6 weeks after implantation in both acute and sub-acute groups (Fig. 4A).

Figure 4 presents the neutrophils and mononuclear cell infiltration at the outer edges of the implanted matrix and muscle fibers growth in A-RM, SA-RM/2w, and SA-RM/6w post-repair. The CD31 staining images of the A-RM and SA-RM/6w groups are shown in Fig. 4C. Based on the images, the matrix induced revascularization 6 weeks after repair.

The quantification of muscle cross-sectional area of all groups was presented in Fig. 5. Consistent with Fig. 3, the TT/6w group showed smaller muscle cross-sectional area compared with TT/2w showing the muscle atrophy in the sub-acute model of RCT. According to Fig. 5A, the cross-sectional areas of the fast muscle fibers in sham/6w and TT/6w groups showed significant differences compared with acute and sub-acute/6w groups. There was no significant difference between acute repair groups (2430 ± 91.99 μm^2 and 2537 ± 92.14 μm^2, for A-RS and A-RM, respectively), and sub-acute repair groups 6 weeks post-repair (2618 ± 92.22 μm^2 and 2724 ± 92.37 μm^2, for SA-RS/6w with SA-RM/6w, respectively). However, SA-RM/2w showed a significant increase compared with SA-RS/2w, SA-RS/6w, A-RS, and A-RM.

Figure 5B shows the quantification of intrafibrillar spaces, also termed gap area for all the groups. The sham and TT groups showed the lowest and the highest percentages of gap area respectively. The A-RM, SA-RS/6w, and SA-RM/6w showed significant differences compared with the TT

Fig. 2 Supraspinatus weight loss in (**A**) acute and (**B**) sub-acute repair groups 2 and 6 weeks after surgery (ns = $P > 0.05$, * = $P \leq 0.05$, ** = $P \leq 0.01$, *** = $P \leq 0.001$, **** = $P \leq 0.0001$)
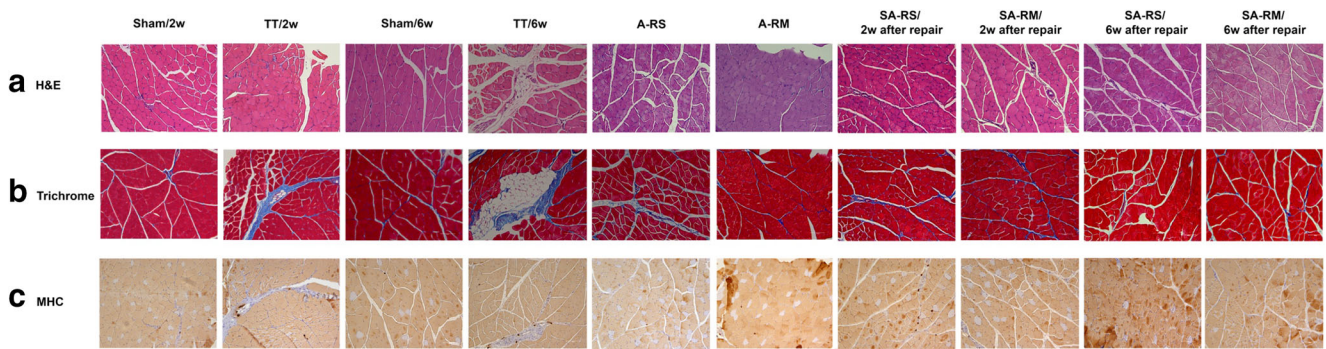
Fig. 3 Histology images of the supraspinatus muscle for both acute and sub-acute groups, (**A**) H&E, (**B**) Masson trichrome staining, and (**C**) immunohistochemistry of myosin heavy chain

group. However, there was no significant difference between the sham group and repair groups with matrices (A-RM and SA-RM/6w).

Discussion

Incorporation of electroactive biomaterials along with topographical cue can facilitate electrical signal transfer in electrically excitable tissues such as skeletal muscle. Studies suggested that electroconductive materials can significantly promote muscle regeneration even without applying external electrical stimulation [4, 44–46]. The potential of aligned PEDOT:PSS/PCL nanofibers to proliferate and differentiate myoblasts was investigated by our group and published elsewhere [4]. Further to the in vitro evaluation, the regenerative ability of the electroconductive matrix to treat RC muscle atrophy was examined in this study. Many patients with torn RC tendons do not visit a physician until several months or even years after the initial injury [47]. Muscle atrophy is a

Fig. 4 Cell infiltration into the matrix after repair. (**A**) Fast muscle fiber staining of acute and sub-acute groups 2 and 6 weeks post-repair; (**B**) H&E staining and Masson trichrome staining of acute group 6 weeks after repair; (**C**) CD31 staining of acute and sub-acute groups 6 weeks post-repair
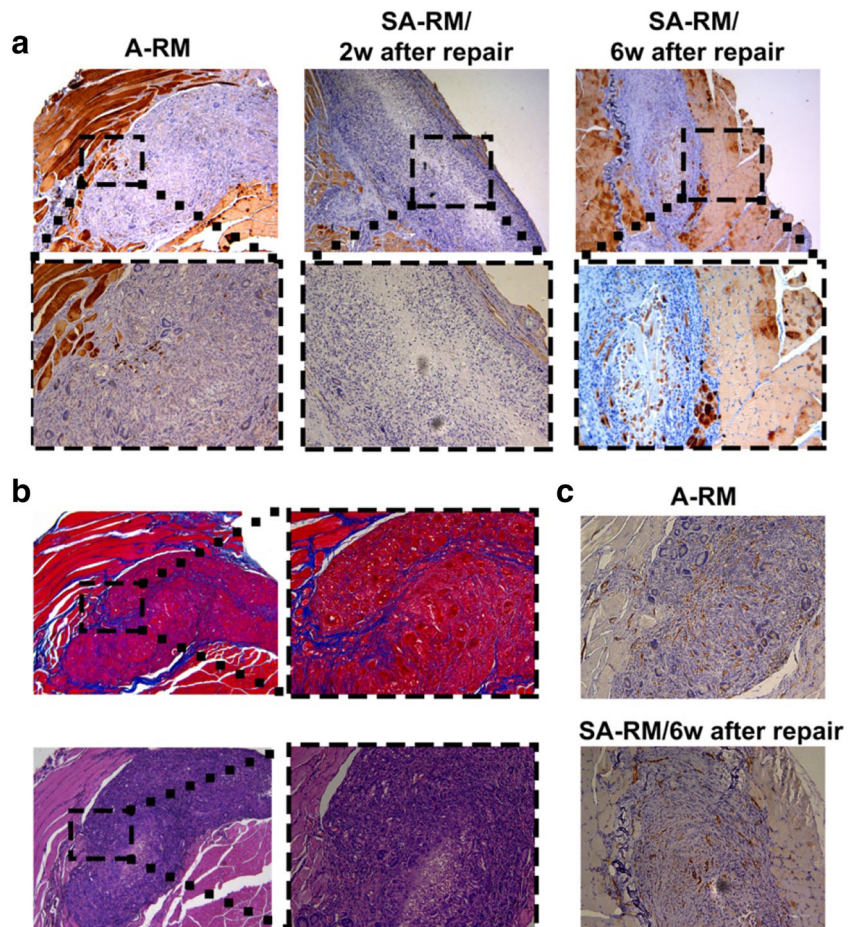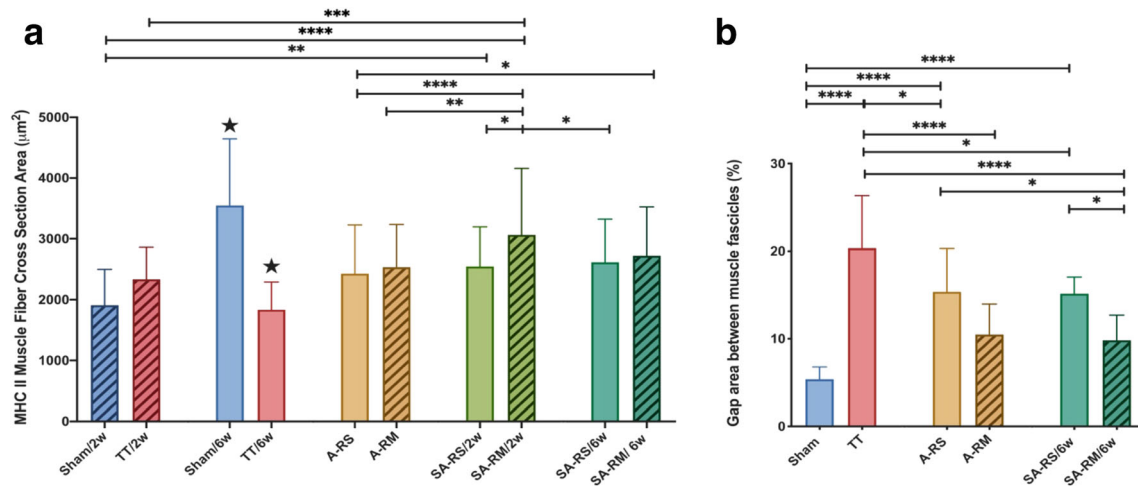
Fig. 5 (A) MHC II muscle fiber cross-sectional area of acute and sub-acute groups 2 and 6 weeks after repair. (B) Gap area between muscle fascicles of acute and sub-acute groups 6 weeks post-surgery (ns =

$P > 0.05$, $* = P \leq 0.05$, $** = P \leq 0.01$, $*** = P \leq 0.001$, $**** = P \leq 0.0001$; black star "★" denote $**** = P \leq 0.0001$ significant difference compared with acute and sub-acute/6w)

commonly observed challenge in sub-acute and chronic RCTs which can occur in the interim between injury and repair. In this study, the clinically relevant rat models of acute and sub-acute RCTs were developed following the tendon repair and implantation of the electroconductive matrix to treat muscle atrophy after successful RC repair. The efficacy of PEDOT:PSS matrix implantation was evaluated compared with the sham group, untreated group (TT), and repair group with suture alone in both acute and sub-acute models. Two and 6 weeks after the repair, the harvested samples were examined by the measurement of supraspinatus muscle weight loss, muscle cross-sectional area, intrafibrillar gap area, and histological changes. These are essential factors in characterizing RC muscle atrophy. Decreased muscle cross-sectional area and muscle mass limit the shoulder motion and muscle post-operative strength, and fail RC tendon repair [48].

The results demonstrated significant changes in supraspinatus muscle mass and muscle cross-sectional area 6 weeks after injury. The high percentage of muscle weight loss in the TT/6w group is consistent with literature showing muscle atrophy after RCT. In both acute and sub-acute models, repaired groups showed significantly less muscle weight loss compared with TT groups. Moreover, the histological results demonstrated the absence of fibrosis in A-RM and SA-RM/6w groups, which indicates the regeneration potential of the electroconductive nanofibrous matrix in both acute and sub-acute models. Moreover, our findings are consistent with clinical results showing that suture repair alone does not reverse muscle degeneration [49, 50].

The immunohistochemistry results demonstrated that MHC type II (fast muscle type) formed the majority of the RC muscle fibers (Fig. 3C). The TT groups showed no MHC I fibers (slow muscle type) 2 and 6 weeks post-surgery. The results were consistent with studies showing slow muscle type

is more vulnerable to atrophy induced by external forces such as denervation as well as immobility because of their higher protein metabolic rate [51]. However, MHC II fibers are more sensitive to cachexia, chronic heart failure, chronic obstructive pulmonary disease, and aging [43]. In both acute and sub-acute repair models, the repair groups were able to recover more type I muscle post-surgery (Fig. 3C). Based on Fig. 5A, TT groups showed statistically significant differences compared with other groups suggesting the efficacy of RC repair in healing muscle atrophy. The study exhibited significantly greater MHC II cross-sectional areas and less muscle atrophy when the repair was augmented with the electroconductive matrix. Moreover, the high percentage of gap area between muscle fascicles in the TT group significantly reduced after matrix implantation.

In both acute and sub-acute groups, the implantation of the engineered matrix reduced the gap area and subsequently improved the muscle atrophy. The study showed that even when there is a delay in surgical repair the electroconductive fibrous matrix can successfully improve the muscle atrophy. The low percentage of gap area and larger muscle cross-sectional area were observed in matrix repaired groups in both acute and sub-acute models, where the matrix acted as a stabilizer for supraspinatus muscle and prevented the gap formation.

Studies reported the mononuclear cell infiltration as an initial response to matrix implantation, which peaks approximately 2 weeks post-surgery and gradually decreases afterward [42]. In our study, cell infiltration was observed 2 weeks post-surgery and continued to decrease by 6 weeks after surgery. At the same time, our results exhibited vascularization on implanted matrices 6 weeks after surgical repair in both acute and sub-acute groups, indicating the potential of the matrix for revascularization. Vascularization is an important step for skeletal muscle regeneration by providing nutrient

delivery and maintaining metabolic conditions [2]. It was reported that RCTs can decrease the vascularity which subsequently correlates with the degree of muscle atrophy [52]. Therefore, improving vascularity may recover RC muscle growth.

The results of acute and sub-acute models demonstrated that the stimulating effects of topographical and electrical cues even without external electrical stimulation can prevent muscle gap formation, increase muscle cross-section area, and subsequently improve muscle atrophy compared with repair groups with suture alone.

Conclusion

In summary, the optimized electroconductive nanofibrous matrix provided synergistic effects of topographical and electrical cues for skeletal muscle tissue engineering. The results of the TT group showed muscle degeneration and atrophy 6 weeks after RCT. However, implantation of the matrix in both acute and sub-acute repairs significantly improved muscle atrophy. The histological results and quantification of muscle fiber cross-sectional area and gap area of repair groups with matrix showed significant improvement compared with TT group and repair groups with suture alone. The study demonstrated the efficacy of electroconductive aligned fibrous matrix in healing the RCT by improving the muscle atrophy in both acute and sub-acute models. Future studies can be conducted to enhance the regenerative potential of the matrix to treat muscle atrophy in RC chronic model with or without external electrical stimulation. Further, the current work only investigated the tissues at the histological level. Other analyses, such as tendon regeneration, biomechanical properties, and fatty infiltration, will be conducted in future studies.

Compliance with Ethical Standards

Competing Interests The authors declare that they have no competing interests.

References

1. Cofield RH, Parvizi J, Hoffmeyer PJ, Lanzer WL, Ilstrup DM, Rowland CM. Surgical repair of chronic rotator cuff tears: a prospective long-term study. JBJS. 2001;83(1):71–7.

2. Ricchetti ET, Aurora A, Iannotti JP, Derwin KA. Scaffold devices for rotator cuff repair. J Shoulder Elb Surg. 2012;21(2):251–65.

3. Saveh-Shemshaki N, Nair LS, Laurencin CT. Nanofiber-based matrices for rotator cuff regenerative engineering. Acta Biomater. 2019;94:64–81.

4. Tang X, Saveh-Shemshaki N, Kan HM, Khan Y, Laurencin CT. Biomimetic electroconductive nanofibrous matrices for skeletal muscle regenerative engineering. Regenerative Engineering and Translational Medicine; 2019. p. 1–10. https://doi.org/10.1007/s40883-019-00136-z.

5. Washington KS, Shemshaki NS, Laurencin CT. The role of nanomaterials and biological agents on rotator cuff regeneration. Regenerative Engineering and Translational Medicine, p. 2020:1–10. https://doi.org/10.1007/s40883-020-00171-1.

6. Kumbar SG, James R, Nukavarapu SP, Laurencin CT. Electrospun nanofiber scaffolds: engineering soft tissues. Biomed Mater. 2008;3(3):034002.

7. Zhao S, Su W, Shah V, Hobson D, Yildirimer L, Yeung KWK, et al. Biomaterials based strategies for rotator cuff repair. Colloids Surf B: Biointerfaces. 2017;157:407–16.

8. Voos JE, Barnthouse CD, Scott AR. Arthroscopic rotator cuff repair: techniques in 2012. Clin Sports Med. 2012;31(4):633–44.

9. Henry P, Wasserstein D, Park S, Dwyer T, Chahal J, Slobogean G, et al. Arthroscopic repair for chronic massive rotator cuff tears: a systematic review. Arthroscopy. 2015;31(12):2472–80.

10. Thangarajah T, et al. Augmentation of rotator cuff repair with soft tissue scaffolds. Orthop J Sports Med. 2015;3(6): 2325967115587495.

11. Gumina S, Borroni M. Classifications of the rotator cuff tears. In: Gumina S, editor. Rotator cuff tear: pathogenesis, evaluation and treatment. Cham: Springer International Publishing; 2017. p. 123–31.

12. Sun Y, Han F, Zhang P, Zhi Y, Yang J, Yao X, et al. A synthetic bridging patch of modified co-electrospun dual nano-scaffolds for massive rotator cuff tear. J Mater Chem B. 2016;4(45):7259–69.

13. Dawson E, Mapili G, Erickson K, Taqvi S, Roy K. Biomaterials for stem cell differentiation. Adv Drug Deliv Rev. 2008;60(2):215–28.

14. Thangarajah T, Henshaw F, Sanghani-Kerai A, Lambert SM, Pendegrass CJ, Blunn GW. Supraspinatus detachment causes musculotendinous degeneration and a reduction in bone mineral density at the enthesis in a rat model of chronic rotator cuff degeneration. Should Elb. 2017;9(3):178–87.

15. Gimbel JA, van Kleunen JP, Mehta S, Perry SM, Williams GR, Soslowsky LJ. Supraspinatus tendon organizational and mechanical properties in a chronic rotator cuff tear animal model. J Biomech. 2004;37(5):739–49.

16. Lundgreen K, Lian OB, Engebretsen L, Scott A. Tenocyte apoptosis in the torn rotator cuff: a primary or secondary pathological event? Br J Sports Med. 2011;45(13):1035–9.

17. Zumstein MA, Lädermann A, Raniga S, Schär MO. The biology of rotator cuff healing. Orthop Traumatol Surg Res. 2017;103(1S): S1–S10.

18. Zumstein MA, et al. The biology of rotator cuff healing. Orthop Traumatol Surg Res. 2017;103(1, Supplement):S1–S10.

19. Gerber C, et al. Neer Award 2007: Reversion of structural muscle changes caused by chronic rotator cuff tears using continuous musculotendinous traction. An experimental study in sheep. J Shoulder Elb Surg. 2009;18(2):163–71.

20. Beeler S, Ek ET, Gerber C. A comparative analysis of fatty infiltration and muscle atrophy in patients with chronic rotator cuff tears and suprascapular neuropathy. J Shoulder Elb Surg. 2013;22(11): 1537–46.

21. Sun Z, Nair LS, Laurencin CT. The paracrine effect of adipose-derived stem cells inhibits IL-1β-induced inflammation in chondrogenic cells through the Wnt/β-catenin signaling pathway. Regen Eng Transl Med. 2018;4(1):35–41.

22. Nelson C, Khan Y, Laurencin CT. Nanofiber/microsphere hybrid matrices in vivo for bone regenerative engineering: a preliminary report. Regen Eng Transl Med. 2018;4(3):133–41.

23. Ifegwu OC, Awale G, Kan HM, Rajpura K, O'Neill E, Kuo CL, et al. Bone regenerative engineering using a protein kinase A-specific cyclic AMP analogue administered for short term. Regen Eng Transl Med. 2018;4(4):206–15.

24. Bowers DT, Brown JL. Nanofibers as bioinstructive scaffolds capable of modulating differentiation through mechanosensitive pathways for regenerative engineering. Regen Eng Transl Med. 2019;5(1):22–9.

25. Heath DE. A review of decellularized extracellular matrix biomaterials for regenerative engineering applications. Regen Eng Transl Med. 2019;5(2):155–66.

26. Clegg JR, Wechsler ME, Peppas NA. Correction to: Vision for functionally decorated and molecularly imprinted polymers in regenerative engineering. Regen Eng Transl Med. 2019;5(4):450.

27. Barajaa MA, Nair LS, Laurencin CT. Bioinspired scaffold designs for regenerating musculoskeletal tissue interfaces: Regenerative Engineering and Translational Medicine; 2019. p. 1–33. https://doi.org/10.1007/s40883-019-00132-3.

28. Qazi TH, Mooney DJ, Pumberger M, Geissler S, Duda GN. Biomaterials based strategies for skeletal muscle tissue engineering:existing technologies and future trends. Biomaterials. 2015;53: 502–21. https://doi.org/10.1016/j.biomaterials.2015.02.110.

29. Bagherzadeh R, Bafqi MSS, Shemshaki NS, Moarref Z, Ghasemi-Nezhad S, Maleki F, et al. Flexible and stretchable nanofibrous piezo-and triboelectric wearable electronics. https://doi.org/10.1088/978-0-7503-2005-4ch7.

30. Bagherzadeh R, Gorji M, Bafgi MS, Saveh-Shemshaki N. Electrospun conductive nanofibers for electronics. In electrospun nanofibers: Woodhead Publishing; 2017. p. 467–519. https://doi.org/10.1016/B978-0-08-100907-9.00018-0.

31. Saveh-Shemshaki N, Latifi M, Bagherzadeh R, Malekshahi Byranvand M, Naseri N, Dabirian A. Synthesis of mesoporous functional hematite nanofibrous photoanodes by electrospinning. Polym Adv Technol. 2016;27(3):358–65.

32. Saveh-Shemshakia N, Latifia M, Bagherzadeh R, Dabirianc A. Functional Fe2O3 Nanofiber photoanodes for photoelectrochemical water splitting application.

33. Saveh-Shemshaki N, Bagherzadeh R, Latifi M. Electrospun metal oxide nanofibrous mat as a transparent conductive layer. Org Electron. 2019;70:131–9.

34. Li WJ, Laurencin CT, Caterson EJ, Tuan RS, Ko FK. Electrospun nanofibrous structure: a novel scaffold for tissue engineering. J Biomed Mater Res. 2002;60(4):613–21.

35. Jiang T, Carbone EJ, Lo KWH, Laurencin CT. Electrospinning of polymer nanofibers for tissue regeneration. Prog Polym Sci. 2015;46:1–24. https://doi.org/10.1016/j.progpolymsci.2014.12.001.

36. Balint R, Cassidy NJ, Cartmell SH. Conductive polymers: towards a smart biomaterial for tissue engineering. Acta Biomater. 2014;10(6):2341–53.

37. Lee JY, Bashur CA, Goldstein AS, Schmidt CE. Polypyrrole-coated electrospun PLGA nanofibers for neural tissue applications. Biomaterials. 2009;30(26):4325–35. https://doi.org/10.1016/j.biomaterials.2009.04.042.

38. Ostrovidov S, Hosseini V, Ahadian S, Fujie T, Parthiban SP, Ramalingam M, et al. Skeletal muscle tissue engineering: methods to form skeletal myotubes and their applications. Tissue Eng B Rev. 2014;20(5):403–36.

39. Gilmore KJ, Kita M, Han Y, Gelmi A, Higgins MJ, Moulton SE, et al. Skeletal muscle cell proliferation and differentiation on poly-pyrrole substrates doped with extracellular matrix components. Biomaterials. 2009;30(29):5292–304.

40. Jun I, Jeong S, Shin H. The stimulation of myoblast differentiation by electrically conductive sub-micron fibers. Biomaterials. 2009;30(11):2038–47.

41. Lee H, et al. Mussel-inspired surface chemistry for multifunctional coatings. Science. 2007;318(5849):426–30.

42. Hyatt JPK, Roy RR, Baldwin KM, Wernig A, Edgerton VR. Activity-unrelated neural control of myogenic factors in a slow muscle. Muscle Nerve. 2006;33(1):49–60.

43. Rui Y, Pan F, Mi J. Composition of muscle fiber types in rat rotator cuff muscles. Anat Rec. 2016;299(10):1397–401.

44. Yang HS, Lee B, Tsui JH, Macadangdang J, Jang SY, Im SG, et al. Electroconductive nanopatterned substrates for enhanced myogenic differentiation and maturation. Adv Healthc Mater. 2016;5(1):137–45.

45. Chen M-C, Sun Y-C, Chen Y-H. Electrically conductive nanofibers with highly oriented structures and their potential application in skeletal muscle tissue engineering. Acta Biomater. 2013;9(3): 5562–72.

46. Du Y, et al. Biomimetic elastomeric, conductive and biodegradable polycitrate-based nanocomposites for guiding myogenic differentiation and skeletal muscle regeneration. Biomaterials. 2018;157:40–50.

47. Lee C, Liu M, Agha O, Kim HT, Liu X, Feeley BT. Beige fibro-adipogenic progenitor transplantation reduces muscle degeneration and improves function in a mouse model of delayed repair of rotator cuff tears. J Shoulder Elb Surg. 2020;29(4):719–27. https://doi.org/10.1016/j.jse.2019.09.021.

48. Chung SW, Kim SH, Tae SK, Yoon JP, Choi JA, Oh JH. Is the supraspinatus muscle atrophy truly irreversible after surgical repair of rotator cuff tears? Clin Orthop Surg. 2013;5(1):55–65.

49. Gladstone JN, Bishop JY, Lo IK, Flatow EL. Fatty infiltration and atrophy of the rotator cuff do not improve after rotator cuff repair and correlate with poor functional outcome. Am J Sports Med. 2007;35(5): 719–28. https://doi.org/10.1177/0363546506297539.

50. Shen P-H, Lien SB, Shen HC, Lee CH, Wu SS, Lin LC. Long-term functional outcomes after repair of rotator cuff tears correlated with atrophy of the supraspinatus muscles on magnetic resonance images. J Shoulder Elb Surg. 2008;17(1):S1–7.

51. Wang Y, Pessin JE. Mechanisms for fiber-type specificity of skeletal muscle atrophy. Curr Opin Clin Nutr Metab Care. 2013;16(3): 243–50.

52. Gigliotti D, Xu MC, Davidson MJ, Macdonald PB, Leiter JRS, Anderson JE. Fibrosis, low vascularity, and fewer slow fibers after rotator-cuff injury. Muscle Nerve. 2017;55(5):715–26.

Regen. Eng. Transl. Med. (2021) 7:1–9

9

Affiliations

Xiaoyan Tang [1,2,3,4] · Nikoo Saveh Shemshaki [1,2,4,5] · Varadraj N. Vernekar [1,2,4] · Anupama Prabhath [1,2,4,5] ·
Emmanuel Kuyinu [1,2,4] · Ho-Man Kan [1,2,4] · Mohammed Barajaa [1,2,4,5] · Yusuf Khan [1,2,3,4,5] · Cato T. Laurencin [1,2,3,4,5,6,7] (iD)

[1] Connecticut Convergence Institute for Translation in Regenerative Engineering, University of Connecticut Health Center, Farmington, CT 06030, USA

[2] Raymond and Beverly Sackler Center for Biomedical, Biological, Physical and Engineering Sciences, University of Connecticut Health Center, Farmington, CT 06030, USA

[3] Department of Materials Science and Engineering, University of Connecticut, Storrs, CT 06269, USA

[4] Department of Orthopaedic Surgery, University of Connecticut Health Center, Farmington, CT 06030, USA

[5] Department of Biomedical Engineering, University of Connecticut, Storrs, CT 06269, USA

[6] Department of Chemical & Biomolecular Engineering, University of Connecticut, Storrs, CT 06269, USA

[7] Department of Craniofacial Sciences, School of Dental Medicine, University of Connecticut Health Center, Farmington, CT 06030, USA